Journal Pre-proof

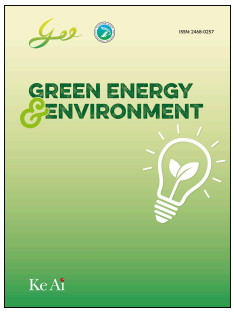

Defect Engineering of TiO_2 for Efficient Photocatalytic Transfer Hydrogenation with Palladium as Cocatalyst and Water as a Hydrogen Source

En Zhao, Jingyuan Su, Hehe Fan, Bing Nan, Lina Li, Haifeng Qi, Weiwei Fang, Wenjun Zhang, Zupeng Chen

PII: S2468-0257(25)00243-2

DOI: https://doi.org/10.1016/j.gee.2025.09.008

Reference: GEE 909

To appear in: *Green Energy & Environment*

Received Date: 10 June 2025

Revised Date: 27 July 2025

Accepted Date: 10 September 2025

Please cite this article as: E. Zhao, J. Su, H. Fan, B. Nan, L. Li, H. Qi, W. Fang, W. Zhang, Z. Chen, Defect Engineering of TiO_2 for Efficient Photocatalytic Transfer Hydrogenation with Palladium as Cocatalyst and Water as a Hydrogen Source, *Green Energy & Environment*, https://doi.org/10.1016/j.gee.2025.09.008.

Defect Engineering of TiO_2 for Efficient Photocatalytic Transfer Hydrogenation with Palladium as Cocatalyst and Water as a Hydrogen Source

En Zhao[1,2], Jingyuan Su[1,2], Hehe Fan[1,2], Bing Nan[3,], Lina Li[3], Haifeng Qi[4], Weiwei Fang[1,2], Wenjun Zhang,[1,2,]* and Zupeng Chen[1,2,]**

[1]National Key Laboratory for the Development and Utilization of Forest Food Resources, Nanjing Forestry University, Nanjing 210037, China

[2]Jiangsu Co-Innovation Center of Efficient Processing and Utilization of Forest Resources, International Innovation Center for Forest Chemicals and Materials, Nanjing Forestry University, Longpan Road 159, Nanjing 210037, China

[3]Shanghai Synchrotron Radiation Facility, Shanghai Advanced Research Institute, Zhangheng Road 293, Shanghai 201204, China

[4]Max Planck-Cardiff Centre on the Fundamentals of Heterogeneous Catalysis FUNCAT, Translational Research Hub, Cardiff University, Maindy Road, Cardiff CF24 4HQ, UK

Graphical abstract

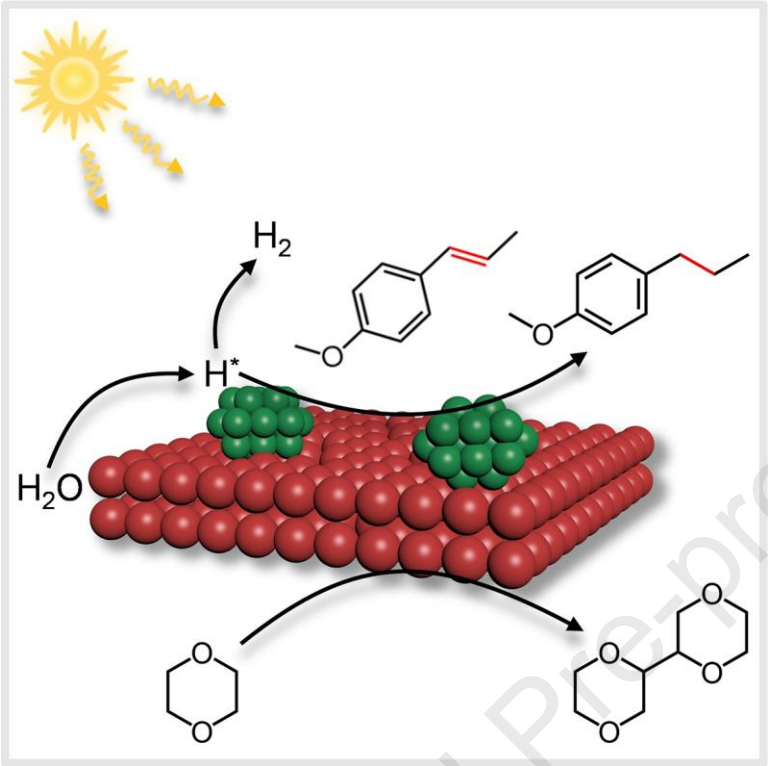

We report an oxygen-defective TiO_2-supported palladium catalyst for efficient photocatalytic transfer hydrogenation using water as the proton source, which exhibits high functional group tolerance and broad substrate applicability, enabling the complete conversion of sixteen substrates.

Defect Engineering of TiO_2 for Efficient Photocatalytic Transfer Hydrogenation with Palladium as Cocatalyst and Water as a Hydrogen Source

En Zhao[1,2], Jingyuan Su[1,2], Hehe Fan[1,2], Bing Nan[3,], Lina Li[3], Haifeng Qi[4], Weiwei Fang[1,2], Wenjun Zhang,[1,2,]* and Zupeng Chen[1,2,]**

[1]National Key Laboratory for the Development and Utilization of Forest Food Resources, Nanjing Forestry University, Nanjing 210037, China

[2]Jiangsu Co-Innovation Center of Efficient Processing and Utilization of Forest Resources, International Innovation Center for Forest Chemicals and Materials, Nanjing Forestry University, Longpan Road 159, Nanjing 210037, China

[3]Shanghai Synchrotron Radiation Facility, Shanghai Advanced Research Institute, Zhangheng Road 293, Shanghai 201204, China

[4]Max Planck-Cardiff Centre on the Fundamentals of Heterogeneous Catalysis FUNCAT, Translational Research Hub, Cardiff University, Maindy Road, Cardiff CF24 4HQ, UK

Keywords. Photocatalysis; Transfer Hydrogenation; Palladium; Defect Engineering; Water Splitting

Abstract. Photocatalytic transfer hydrogenation using water as the proton source has emerged as an attractive and green approach for the catalytic reduction of unsaturated bonds. Herein, we report an oxygen-defective TiO_2-supported palladium catalyst (Pd-TiO_2-O_v) for efficient photocatalytic water-donating transfer hydrogenation of anethole towards 4-n-propylanisole in a high yield of 99.9%, which is significantly higher compared to the pristine TiO_2-supported palladium catalyst (Pd-TiO_2, 74%). The enhanced performance is ascribed to the presence of oxygen vacancies, which facilitate light absorption and suppress the recombination of photogenerated electron-hole pairs. Furthermore, the Pd-TiO_2-O_v is versatile in hydrogenating various alkene substrates including those with hydroxyl, ether, fluoride, and chloride functional groups in full conversion, thus offering a green method for transfer hydrogenation of alkenes. This study provides new insights and advances in current hydrogenation technology with water as the proton source.

1. Introduction

Enormous attention has been devoted to the pursuit of artificial photosynthesis for solar-to-chemical energy conversion with minimal environmental impact.[1-3] Most of these studies have focused on photocatalytic hydrogen evolution,[4-6] since hydrogen is one of the most promising fuels with high energy density and no pollutants are produced during its combustion. Globally, more than 50 million tons of hydrogen are consumed annually for the agricultural, chemical, and pharmaceutical industries.[7] However,

flammable hydrogen suffers from low bulk density under ambient conditions, which poses serious challenges for its storage and transport.[8] Solar-driven organic conversion has emerged as a possible alternative (*e.g.*, hydrogenation,[9, 10] oxidation,[11] and coupling[12, 13]) that could produce value-added products for convenient storage and transportation, thus providing new avenues for the efficient utilization of solar energy.

The hydrogenation of alkenes is among the most fundamental transformations in organic synthesis, with industrial applications varying from fine chemicals engineering to pharmaceutical manufacturing.[14-16] Conventional thermal hydrogenation is typically conducted at a high temperature and pressure as well as using pressurized H_2 as the proton source, which is potentially risky and energy-intensive.[17] Furthermore, elaborate high-pressure resistant equipment is usually required. Substitutionally, the chemical transformation can be accomplished by photocatalytic transfer hydrogenation to develop green and sustainable chemical production processes, which involves the hydrogen transfer from a liquid hydrogen donor (*e.g.*, water and alcohol) to a target molecule.[18-20] Recently, Studer *et al.* demonstrated water activation with a photocatalytic phosphine-mediated radical process for the hydrogenation of alkenes under mild conditions.[9] Xu *et al.* employed a carbon nitride-supported platinum nanoparticle photocatalyst for the proton addition of the C=C bond using water as the hydrogen source.[21] The single-atom catalysts also exhibited enormous potential in photocatalytic water-donating transfer hydrogenation.[20, 22] However, unsatisfactory

catalytic activity and poor substrate tolerance remained to be resolved. Moreover, the existing catalytic systems required the addition of hole scavengers (*e.g.*, methanol, triethanolamine, triethylamine, and Na_2SO_3), which led to a waste of resources and hindered the development of photocatalysis.

Herein, we reported an oxygen-defective TiO_2-supported palladium catalyst (Pd-TiO_2-O_v) for efficient photocatalytic transfer hydrogenation using water as the proton source. Comprehensive characterizations including X-ray photoelectron spectroscopy (XPS), electron paramagnetic resonance (EPR), and transmission electron microscopy (TEM) verified the formation of oxygen vacancies. The resulting Pd-TiO_2-O_v exhibited superior catalytic performance for transfer hydrogenation of anethole using water as a proton source with a 99.9% yield of 4-n-propylanisole formation. The enhanced preformation could be ascribed to the existence of oxygen vacancies, which promoted light absorption and prevented the recombination of the photogenerated electron-hole pairs. Isotopic-labeling experiments confirmed the hydrogenation mechanism using active hydrogen intermediates (H*) from water splitting in the reduction end, and EPR experiments verified that 1,4-dioxane was oxidized to generate 2,2'-Bi(1,4-dioxane) at the oxidation end. Finally, the catalytic system demonstrated high functional group tolerance and broad substrate applicability with full conversion.

2. Experimental section

Photocatalysts synthesis

To synthesize TiO_2-O_v, 0.5 g Commercial TiO_2 (P25) was reduced at 773 K (5 K min^{-1} ramp rate) for 3 h under a 10% H_2/Ar atmosphere. To prepare Pd-TiO_2 or Pd-TiO_2-O_v, a certain amount of $PdCl_2$ solution (2 mg mL^{-1}) was added to deionized water (50 mL), then 0.5 g support was dispersed in the above $PdCl_2$ aqueous solution with vigorous stirring in an oil bath at 90°C until dry. Samples with 0.5, 1.0, 1.5, and 3.0 wt.% Pd loading were obtained with the addition of $PdCl_2$ solution (2 mg mL^{-1}) of 2.1, 4.2, 6.4, and 12.9 mL. The collected solid powders were further dried at 353 K overnight. Finally, samples were calcined at 673 K (5 K min^{-1} ramp rate) for 5 h under a 10% H_2/Ar atmosphere.

Characterization methods

The palladium content in the photocatalysts was tested by an Inductively Coupled Plasma Optical Emission Spectrometer (Varian ICP-OES 720). Powder X-ray diffraction (XRD) patterns were performed using Ultima IV X-ray diffractometer using Cu Kα radiation (λ = 1.541841 Å). X-ray photoelectron spectroscopy (XPS) measurements were undertaken on a Thermo ESCALAB 250XI with an Al anode (Al-Kα = 1486.6 eV), in which all spectra were referenced to the C 1s peak at 284.8 eV. The XPS spectra were analyzed by Avantage software, in which the full width at half maximum (FWHM) between the Pd $3d_{3/2}$ and Pd $3d_{5/2}$ peaks was fixed. UV-vis diffuse

reflectance spectra (DRS) were conducted in a Lambda 950 spectrophotometer with $BaSO_4$ as the reflectance standard. Transmission electron microscopy (TEM), high angle annular dark-field scanning transmission electron microscopy (HAADF-STEM), and energy-dispersive spectroscopy (EDS) images were obtained by a JEM 2100F TEM/STEM. Scanning electron microscopy (SEM) images were acquired on a Hitachi S-4800 instrument. The photoluminescence (PL) measurements were recorded using Hitachi F4600 spectrophotometer under 370 nm excitation. The time-resolved photoluminescence (TRPL) spectra were monitored at 530 nm under 375 nm excitation using FLS980. The electron paramagnetic resonance (EPR) measurements were conducted on a Bruker EMX plus instrument. The synchrotron radiation measurement was recorded on the BL14W1 beamline of the Shanghai Synchrotron Radiation Facility (SSRF) operated at 3.5 GeV under "top-up" mode with a constant current of 240 mA under fluorescence mode.

Photoelectrochemical measurements

Electrochemical measurements were performed using a CHI760E electrochemical workstation (Chenhua Instrument Co. Ltd., Shanghai, China) with a standard three-electrode cell, in which the prepared electrode, a platinum foil, and Ag/AgCl (saturated KCl) acted as the working, counter, and reference electrode, respectively, and the three-electrodes were soaked in a 0.2 mol L^{-1} electrolyte solution of sodium sulfate. The working electrodes were prepared as follows: catalysts (5 mg) and Nafion

solution (0.05 mL) were added to ultrapure water (0.45 mL) under sonication for 1 h. Then, the above slurry (0.010 mL) was dropped onto a $\pi \times 0.6 \times 0.6$ cm^2 fluorine-tin oxide (FTO) glass electrode and dried at 353 K. The transient photocurrent responses were performed using a 300 W xenon lamp with a 365 nm filter at 0 V (vs. Ag/AgCl). The electrochemical impedance spectroscopies (EIS) were carried out in frequencies from 10^5 to 10^{-1} Hz with an amplitude of 5 mV at 0 V (vs. Ag/AgCl). Mott-Schottky analysis was recorded over a potential range from −0.7 to 0.7 V (vs. Ag/AgCl) and 5 mV perturbation signal at different frequencies (2000 and 3000 Hz).

Photocatalytic activity test

The photocatalytic water-donating transfer hydrogenation was performed in a 12 mL Schlenk reactor. In a typical process, photocatalyst (5 mg) and ultrapure water (2 mL) were added to the reactor and sonicated for 1 min. Subsequently, 1,4-dioxane (5 mL) and substrate (0.1 mmol) were added, then the reactor was purged with N_2. Afterward, the reactor was irradiated by a 300 W xenon lamp with a 365 nm filter from a fixed distance of 10 cm, with an irradiation area of approximately 9.7 cm^2. The irradiance of the LED lamp is 112.8 mW cm^{-2}. After the irradiation, the liquid was collected and analyzed by GC-MS (Shimadzu QP2020 NX) using acetophenone as an internal standard. Four concentration gradients of standard solutions for the target analyte were prepared (Figure S17-S18). For the recyclability test, the catalysts after the reaction were directly reused in the next reaction cycle.

The scale-up reaction was performed in a 50 mL Schlenk reactor. Photocatalyst (0.1 g) and ultrapure water (10 mL) were added to the reactor and sonicated for 1 min. Subsequently, 1,4-dioxane (25 mL) and substrate (0.5 g) were added, then the reactor was purged with N_2. The reactor was irradiated for 10 h using a 300 W xenon lamp with a 365 nm filter.

Calculation of yield (Y):

$$Y = \frac{\text{moles of substrate converted to form product}}{\text{moles of initial substrate}} \times 100\%$$

3. Results and discussion

Physicochemical properties

The Pd-TiO_2-O_v with a Pd content of 1.03 wt.% as determined by the inductively coupled plasma optical emission spectrometer (ICP-OES) (Table S1), was synthesized directly by impregnating $PdCl_2$ solution into an H_2-pretreated commercial TiO_2 (P25) following a calcination treatment in H_2/Ar atmosphere (details in Supporting Information). For comparison, the defect-free Pd-TiO_2 was prepared using the same method, except for the direct use of P25. The X-ray diffraction (XRD) pattern of TiO_2-O_v was the same as that of P25 (Figure S1), indicating that the H_2-pretreatment did not affect the intrinsic crystal structure of the P25. Noted that the diffraction peaks of metallic Pd at 39.9 (111) and 45.3° (200) could be observed when the Pd content was above 1 wt.%. The overall morphology and microstructure of TiO_2-O_v and Pd-TiO_2-O_v were then characterized by scanning electron microscopy (SEM), transmission electron

microscopy (TEM), and scanning transmission electron microscopy (STEM). Specifically, irregular TiO_2 particles were observed in TiO_2-O_v and Pd-TiO_2-O_v by TEM (Figure 1a-b) and SEM images (Figure S2), and the corresponding energy dispersive X-ray spectroscopy (EDS) analysis demonstrated the homogeneous distribution of Pd, Ti, and O throughout the Pd-TiO_2 and Pd-TiO_2-O_v (Figure S3-4). Furthermore, the lattice spacing of the (111) plane of Pd (0.23 nm) was observed by the high-resolution (HR) TEM image of Pd-TiO_2-O_v (Figure 1c). As shown in the STEM images of TiO_2-O_v and Pd-TiO_2-O_v (Figure 1d-e), the average sizes of the Pd nanoparticles (NPs) in TiO_2-O_v and Pd-TiO_2-O_v were revealed to be 4.11 and 3.84 nm

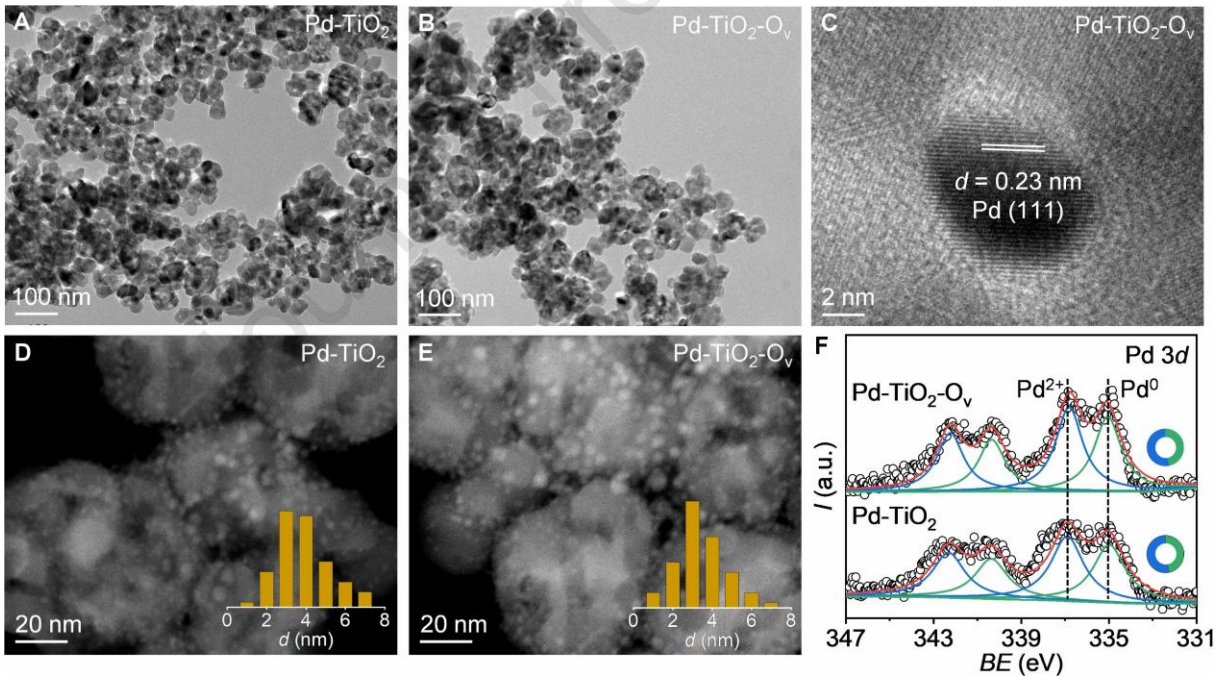

Figure 1. (HR) TEM images of (a) Pd-TiO_2 and (b-c) Pd-TiO_2-O_v. HAADF-STEM (insets, size distribution of Pd nanoparticles) images of (d) Pd-TiO_2 and (e) Pd-TiO_2-O_v. (f) Pd 3*d* XPS spectra of Pd-TiO_2 and Pd-TiO_2-O_v. The donut plot in (f) indicates the relative distribution of Pd^0 (green) and Pd^{2+} (blue).

(insets), respectively. Moreover, the chemical states of Pd species in the catalysts were studied by X-ray photoelectron spectroscopy (XPS) (Figure 1f). Two types of Pd species were observed in the Pd 3*d* spectra of Pd-TiO_2 and Pd-TiO_2-O_v, which could be assigned to Pd^0 (335.0 eV) and Pd^{2+} (336.7 eV) based on formal charges. As shown in the donut plots (insets), the ratio of Pd^{2+}/Pd^0 in Pd-TiO_2 (1.12) and Pd-TiO_2-O_v (1.14) is almost identical, indicating that the change in the carrier has no effect on the loading of Pd metal.

Considering the variation in surface defect during the H_2-pretreated process, a comprehensive investigation into the content of oxygen vacancy was investigated using O 1*s* and Ti 2*p* XPS, electron paramagnetic resonance (EPR), and HRTEM analyses. The O 1*s* XPS of Pd-TiO_2 and Pd-TiO_2-O_v were collected (Figure 2a), showing two main peaks at 529.9 and 532.2 eV that could be assigned to the lattice oxygen of Ti−O bond and the adsorbed oxygen on the surface, respectively. The content of adsorbed O in Pd-TiO_2-O_v increased significantly compared to that of Pd-TiO_2 due to the presence of more surface oxygen vacancies (insets in Figure 2a). In addition, the Ti 2*p* spectrum of Pd-TiO_2-O_v demonstrated decreased binding energies when compared with Pd-TiO_2, providing clear evidence for the lower valence state of Ti resulting from the presence of oxygen vacancies and the stronger interaction between the Pd species and TiO_2-O_v (Figure 2b). The EPR measurements were further employed to explore the surface defects. As shown in Figure 2c, Pd-TiO_2-O_v exhibited relatively stronger EPR signal

intensities at $g \approx 2.003$ than that of Pd-TiO_2 under both light and dark conditions, implying the higher number of surface oxygen vacancies in Pd-TiO_2-O_v than Pd-TiO_2.[23] Furthermore, the analysis by HRTEM revealed the generation of defective surface layers in the H_2-pretreated Pd-TiO_2-O_v, which was not observed in Pd-TiO_2 (Figure S5).

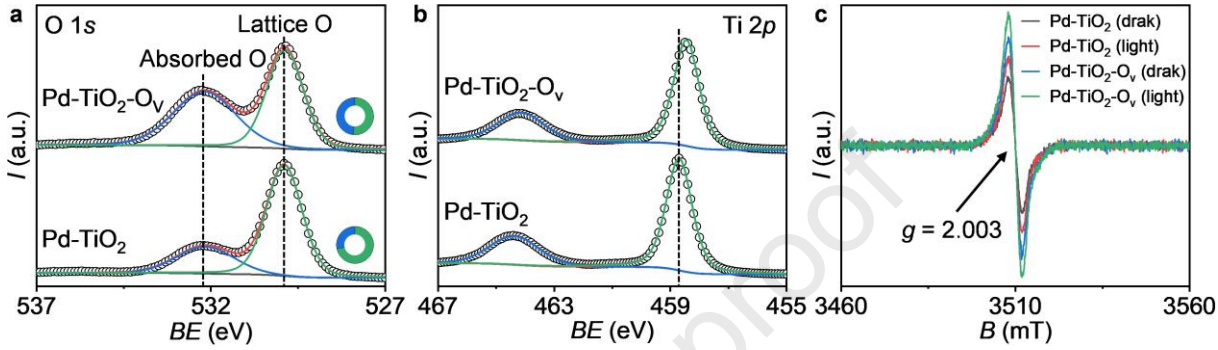

Figure 2. XPS of the (a) O 1*s* and (b) Ti 2*p* spectra of Pd-TiO_2 and Pd-TiO_2-O_v. The donut plot in (a) indicates the relative distribution of lattice oxygen (green) and adsorbed O (blue). (c) EPR spectra of Pd-TiO_2 and Pd-TiO_2-O_v under dark and light conditions.

Since the aforementioned results conclusively demonstrated the defective surface structure in Pd-TiO_2-O_v, the X-ray absorption fine structure (XAFS) measurement was further conducted to analyze the coordination environments and electronic structure of Pd species on TiO_2-O_v. X-ray absorption near edge structure (XANES) result showed that the absorption edge of Pd-TiO_2-O_v is located between that of the Pd foil and PdO, but closer to the Pd foil (Figure S6a), suggesting that the oxidation state of $Pd^{\delta+}$ ($0 < \delta < 2$) species, in line with the results of XPS analysis. Moreover, the Fourier-transformed (FT) k^2-weighted Pd *K*-edge extended X-ray absorption fine structure (EXAFS) analysis in the *R* space of the Pd-TiO_2-O_v showed one main peak at 2.50 Å (Figure S6b),

attributing to the metallic Pd−Pd scattering. The EXAFS fitting manifests that the coordination number of Pd−Pd is 10.1±1.3 with bond lengths of 2.73±0.01 Å (Figure S6c and Table S2). The results indicated that the Pd species were dispersed on the TiO_2 in the form of well-crystallized nanoparticles.

Photoelectrochemical properties

The optical properties and band structures of Pd-TiO_2 and Pd-TiO_2-O_v were analyzed by UV-visible diffuse reflectance spectroscopy (UV-vis DRS). As shown in Figure 3a, the formation of oxygen vacancies increased the light absorption of Pd-TiO_2-O_v over the entire wavelength range. The bandgaps (E_g) of Pd-TiO_2 and Pd-TiO_2-O_v were calculated to be 3.18 and 3.20 eV according to the Tauc plots, respectively (Figure 3b). Then, the Mott-Schottky (M-S) plots were performed to acquire the conduction band (E_{CB}) positions of Pd-TiO_2 (-1.07 eV vs. Ag/AgCl) and Pd-TiO_2-O_v (-1.06 eV vs. Ag/AgCl) (Figure S7), which corresponded to -0.47 and -0.46 eV (vs. reversible hydrogen electrode (RHE)), respectively. Then, the valence band (E_{VB}) positions could be further calculated to be 2.71 and 2.74 eV for Pd-TiO_2 and Pd-TiO_2-O_v, respectively. Thereafter, their band gap diagrams could be schematically plotted (Figure S8). To study the charge transfer process, electrochemical impedance spectroscopy (EIS) measurements were conducted. As shown in Figure 3c, Pd-TiO_2-O_v presented a smaller EIS radius than Pd-TiO_2, illustrating a lower interface electron-transfer resistance. Additionally, the transient photocurrent experiments showed that Pd-TiO_2-O_v possesses

a faster photocurrent response and a higher photocurrent density under irradiation than Pd-TiO_2 (Figure 3d), indicating the effective promotion of the separation of photogenerated electron-hole pairs. The mobility of photogenerated electron-hole pairs was further investigated by the steady-state photoluminescence (PL) spectra. As shown in Figure 3e, the Pd-TiO_2-O_v sample showed a weaker PL emission peak, which might be due to the presence of more structural defects. Moreover, time-resolved photoluminescence (TRPL) spectra (Figure 3f) exhibited that the average lifetime of the photogenerated charges of Pd-TiO_2-O_v (2.16 ns) was shorter than that of Pd-TiO_2 (2.85 ns), which suggested that photogenerated charges in Pd-TiO_2-O_v were transferred to certain favorable localized states (*e.g.*, surface defects), thus facilitating the

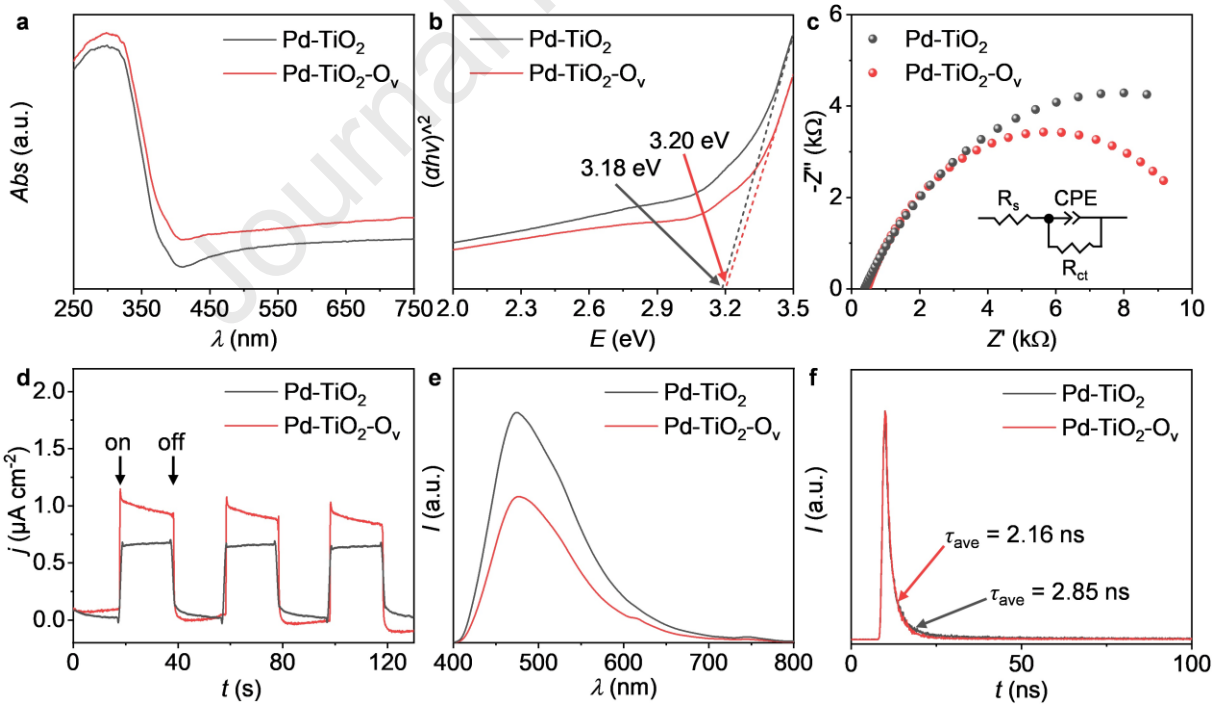

Figure 3. (a) UV-vis absorption spectra, (b) Tauc plots, (c) electrochemical impedance spectra, (d) transient photocurrent responses, (e) solid-state PL spectra, and (f) time-resolved PL spectra of Pd-TiO_2 and Pd-TiO_2-O_v.

separation of photogenerated electron-hole pairs. These results manifested that the presence of oxygen vacancies could enhance light absorption and promote the separation and migration of photogenerated electron-hole pairs, which could facilitate the resulting reactivity.

Photocatalytic performance

The catalytic performance of the prepared photocatalysts was initially evaluated in the water-donating photocatalytic transfer hydrogenation of biomass-derived anethole without sacrificial agents or additives (Figure 4a). As shown in Figure 4b, Pd-TiO_2-O_v exhibited a higher yield of 4-*n*-propylanisole formation (99.9%) compared to that of Pd-TiO_2 (74%), whereas both TiO_2-O_v and TiO_2 were inactive for the reaction. The effect of the Pd content was then evaluated over TiO_2-O_v (Figure S9a). Compared to the inert TiO_2-O_v, the introduction of a small amount of palladium (0.51 wt.%) could significantly promote the photocatalytic transfer hydrogenation, showing a 37% yield of 4-*n*-propylanisole formation. The yield could increase to 59% in the case of Pd-TiO_2-O_v with 1.03 wt.% Pd species. Although further increasing Pd content to 1.3 and 2.53 wt.% could steadily improve the yield of 4-*n*-propylanisole to 60 and 72%, respectively, the metal utilization efficiency decreased significantly (Figure S9b). Therefore, the Pd-TiO_2-O_v with a Pd content of 1.03 wt.% was selected as the optimal catalyst for the subsequent studies. The control experiments revealed that no hydrogenated product (*i.e.*, 4-*n*-propylanisole) could be observed in the dark, without a

catalyst or H_2O (Figure 4c), suggesting the indispensable roles of these conditions. Noted that a small amount of 4-*n*-propylanisole (1.4%) was observed without the presence of 1,4-dioxane, indicating the possibility of transfer hydrogenation in pure water. Furthermore, the recyclability of the Pd-TiO_2-O_v was examined in a stability test (Figure 4d), exhibiting a slight decay in the yield after five consecutive reaction runs, which should be due to the non-negligible metal leaching (Table S1, from 1.03 to 0.88 wt.%). Further post-analysis of the used catalyst by HAADF-STEM revealed no aggregation of the Pd NPs (an average size of 3.61 nm) (Figure S10).

Afterward, the amount of hydrogen evolution was measured during the transfer hydrogenation of anethole under optimal reaction conditions. 13.4 μmol of hydrogen protons were employed for hydrogen evolution. However, there were approximately 200 μmol of protons for transfer hydrogenation. Therefore, the apparent quantum efficiencies (AQEs) for transfer hydrogenation and hydrogen evolution were 0.72% and 0.05%, respectively, suggesting that the dominating (~93.7%) of the photogenerated hydrogen protons have been utilized for the transfer hydrogenation processes. The Pd-TiO_2-O_v was then demonstrated on a gram scale with the potential for large-scale applications, reaching a 99.9% yield of 4-*n*-propylanisole (Figure S11). Furthermore, we evaluated the photocatalytic transfer hydrogenation performance using outdoor sunlight as the light source (Figure S12). The target product was obtained with a yield of 56.1% under 10 h of solar irradiation, which confirms that our strategy can

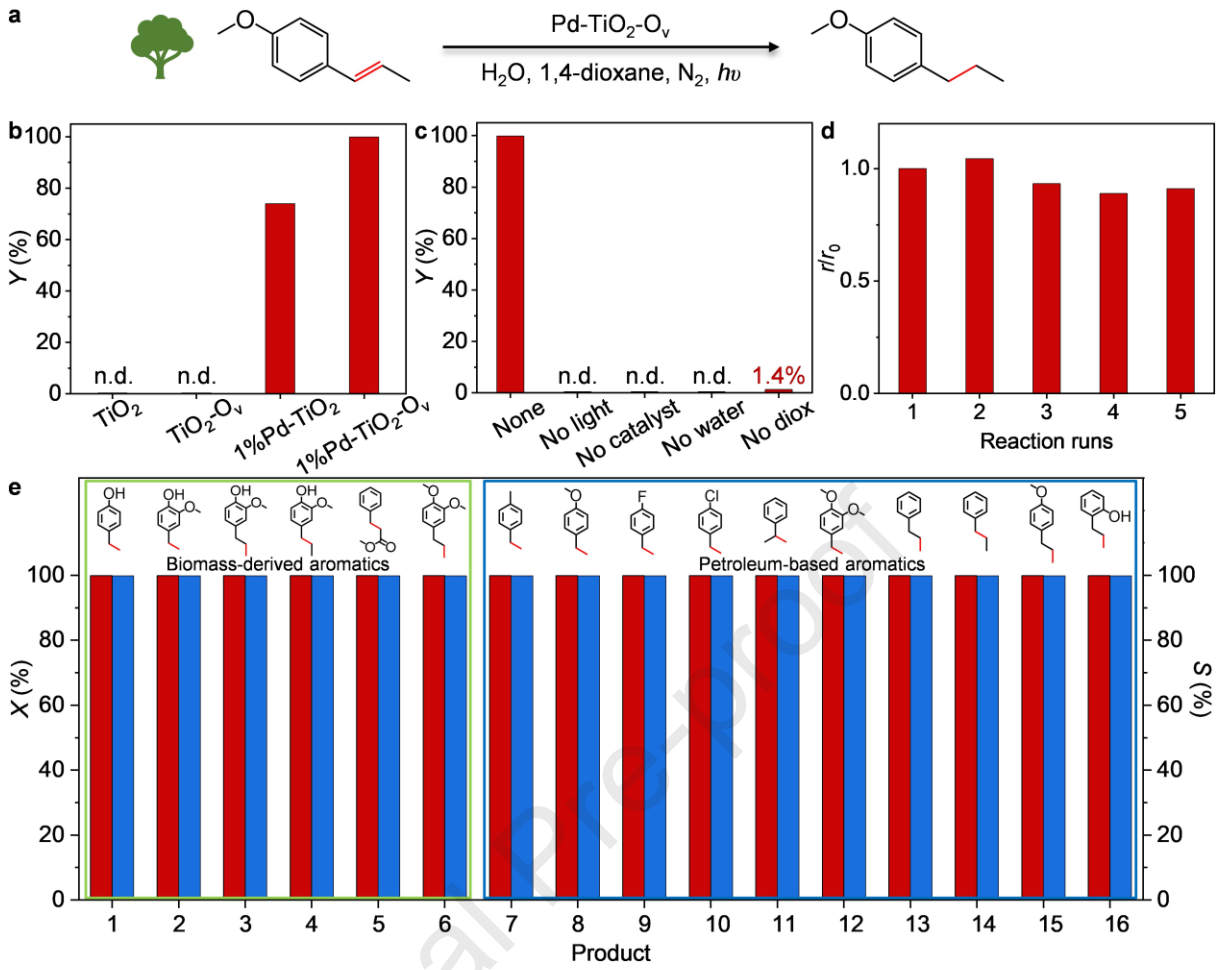

Figure 4. (a) Illustration of the photocatalytic water-donating transfer hydrogenation using anethole as a model substrate. Standard reaction conditions: catalyst (5 mg), anethole (0.1 mmol), ultrapure water (2 mL), 1,4-dioxane (5 mL), reaction time (140 min), 300 W Xenon lamp with 365 nm filter, and N_2 atmosphere. n.d. = not detected. (b) Photocatalytic water-donating transfer hydrogenation over different photocatalysts under standard conditions. (c) Photocatalytic water-donating transfer hydrogenation under various conditions. (d) Reusability testing of Pd-TiO_2-O_v. The stability test was performed under the standard reaction conditions except for a reaction time of 50 min. (e) Reaction scope of the photocatalytic water-donating transfer hydrogenation reactions under the standard reaction conditions except for different reaction times: 3 h (entries 1-5 and 7-16) and 4 h (entry 6).

effectively utilize renewable solar energy, further highlighting its potential for sustainable and large-scale applications. The reaction scope and effectiveness of the prepared Pd-TiO2-Ov in photocatalytic water-donating transfer hydrogenation reactions were further investigated. Broad substrate scope for the hydrogenation of aromatic olefins was investigated (Figure 4e), including biomass-derived chemicals (entries 1-6) and petrochemicals (entries 7-16). Remarkably, all sixteen substrates showed 100% conversion, resulting in the complete hydrogenation of olefins. The result not only validated the robustness and high activity of our developed catalytic system but also implied broad applicability and potential in complex organic synthesis.

Mechanism analysis

The photocatalytic water-donating transfer hydrogenation mechanism was first investigated by isotope-labeling experiments. As shown in Figure 5a and Figure S13, a molecular ion peak of the 4-*n*-propylanisole at m/z = 150 was detected by gas chromatography-mass spectrometry (GC-MS) after the photocatalytic transfer hydrogenation in H_2O using anethole (m/z = 148) as substrate (Figure S14). Rather, a deuterated 4-*n*-propylanisole product (m/z = 152) was discovered when the reaction was conducted in D_2O (Figure S15), pointing to the direct water-donating protonation of anethole at the reduction end. Moreover, the production of 2,2'-bi(1,4-dioxane) was observed by GC-MS (Figure S16), which might be caused by the oxidation of 1,4-dioxane at the oxidation end. Furthermore, EPR experiments were also employed to

study the reaction intermediate using 5,5-dimethyl-1-pyrroline N-oxide (DMPO) as the radical trapping agent. As shown in Figure 5b, the absence of the EPR signal in the dark indicated that the constituents of the standard reaction system remained inert with respect to DMPO in the absence of light-induced activation or other perturbing factors. While under UV light irradiation, the typical EPR signals of carbon radicals were

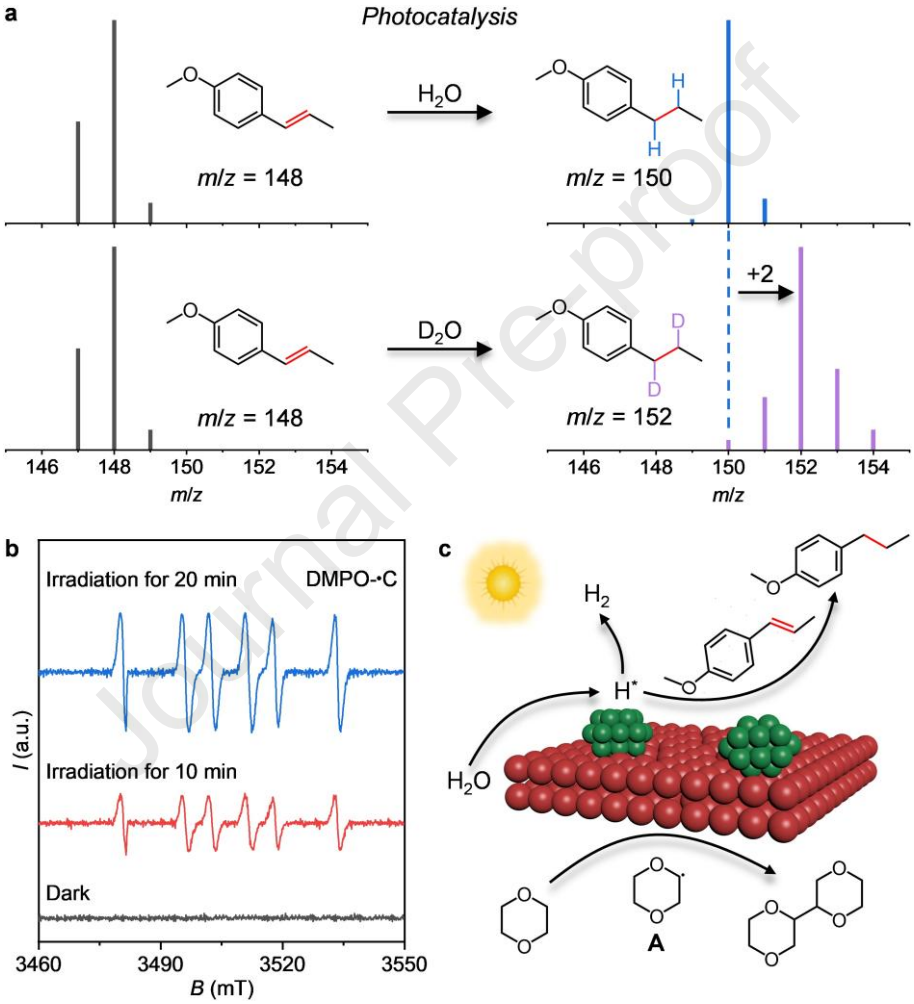

Figure 5. (a) Mass spectra of the liquid products from the photocatalytic water-donating transfer hydrogenation in H_2O and D_2O, respectively. (b) EPR spectra of carbon radical in standard reaction system captured by DMPO. (c) Proposed mechanism of photocatalytic water-donating transfer hydrogenation reaction catalyzed by Pd-TiO_2-O_v.

observed and the intensity increased with time.[24] Based on the above experimental results, a possible mechanism for the photocatalytic water-donating transfer hydrogenation process was proposed (Figure 5c). At the reduction end, water is photolyzed to produce active hydrogen intermediates (H*), which are subsequently adsorbed onto the surface of metal species for the hydrogenation of organics. Meanwhile, a small amount of H* inevitably generates H_2 (detected by gas chromatography). Moreover, 1,4-dioxane is oxidized to form an intermediate (**A**) at the oxidation end, which is subsequently coupled to form 2,2'-Bi(1,4-dioxane), in agreement with previous literature.[25]

4. Conclusions

In summary, we have demonstrated that Pd nanoparticles-supported TiO_2 with oxygen vacancies (Pd-TiO_2-O_v) could facilitate the photocatalytic water-donating transfer hydrogenation. The formation of oxygen vacancies was verified through multiple techniques including X-ray photoelectron spectroscopy (XPS), electron paramagnetic resonance (EPR), and high-resolution transmission electron microscopy (HRTEM). Photoelectrochemical characterizations have revealed that the defect structure in Pd-TiO_2-O_v could enhance light absorption and suppress the rapid recombination of photogenerated electron-hole pairs, consequently bolstering the photocatalytic performance. Notably, Pd-TiO_2-O_v exhibited remarkable performance in the transfer hydrogenation of anethole. It achieved a high yield of 4-*n*-propylanisole formation

(99.9%) that was 1.4 times higher than that of Pd-TiO_2 (74%) within a simple, environmentally friendly, and cost-effective reaction system composed solely of water and 1,4-dioxane. By employing isotope-labeling techniques and EPR measurements, a possible mechanism was proposed, in which1,4-dioxane undergoes oxidation to yield 2,2'-bi(1,4-dioxane), while the aromatic alkene is hydrogenated by the active hydrogen intermediates (H*) generated from water splitting. Moreover, the strategy presented herein enabled the efficient transfer hydrogenation of diverse aromatic olefins including representative petrochemicals and biomass-derived chemicals, thus offering a sustainable approach to the synthesis of alkanes. These findings offer invaluable guidance for developing a diverse array of clean and non-polluting organic reactions. In these reactions, water can be effectively harnessed as either a hydrogen source or an oxygen source.

CRediT authorship contribution statement

En Zhao: Writing-original draft, Methodology, Investigation, Formal analysis, Data curation. Jingyuan Su: Methodology, Investigation, Formal analysis. Hehe Fan: Methodology, Investigation, Formal analysis. Bing Nan: Methodology, Investigation, Formal analysis. Lina Li: Methodology, Investigation, Formal analysis. Weiwei Fang: Writing review & editing, Methodology, Formal analysis. Wenjun Zhang: Writing-review & editing, Methodology, Formal analysis, Data curation. Zupeng Chen: Writing review & editing, Supervision, Funding acquisition, Conceptualization.

Declaration of competing interest

The authors declare no competing interests.

Acknowledgments

This work was supported by the National Key Research and Development Program of China (2023YFD2200505), National Natural Science Foundation of China (22202105), Natural Science Foundation of Jiangsu Higher Education Institutions of China (21KJA150003), and the Innovation and Entrepreneurship Team Program of Jiangsu Province (JSSCTD202345).

Appendix A. Supplementary data

Supplementary data to this article can be found online at https://doi.org/XXX.

References

1. J. Gong, C. Li and M. R. Wasielewski, Chem. Soc. Rev. 48 (2019) 1862-1864.
2. X. Wu, N. Luo, S. Xie, H. Zhang, Q. Zhang, F. Wang and Y. Wang, Chem. Soc. Rev., 2020, 49, 6198-6223.
3. Q. Wang and K. Domen, Chem. Rev. 120 (2019) 919-985.
4. M. Xiao, L. Zhang, B. Luo, M. Lyu, Z. Wang, H. Huang, S. Wang, A. Du and L. Wang, Angew. Chem. Int. Edit. 59 (2020) 7230-7234.
5. H. Nishiyama, T. Yamada, M. Nakabayashi, Y. Maehara, M. Yamaguchi, Y. Kuromiya, Y. Nagatsuma, H. Tokudome, S. Akiyama, T. Watanabe, R. Narushima, S. Okunaka, N. Shibata, T. Takata, T. Hisatomi and K. Domen, Nature 598 (2021) 304-307.
6. L. Wu, F. Su, T. Liu, G.-Q. Liu, Y. Li, T. Ma, Y. Wang, C. Zhang, Y. Yang and S.-H. Yu, J. Am. Chem. Soc. 144 (2022) 20620-20629.
7. T. Uekert, M. F. Kuehnel, D. W. Wakerley and E. Reisner, Energy Environ. Sci. 11 (2018) 2853-2857.
8. X. Zou and Y. Zhang, Chem. Soc. Rev. 44 (2015) 5148-5180.
9. J. Zhang, C. Mück-Lichtenfeld and A. Studer, Nature 619 (2023) 506-513.

10. F. Arcudi, L. Đorđević, N. Schweitzer, S. I. Stupp and E. A. Weiss, Nat. Chem. 14 (2022) 1007-1012.
11. P. Xie, J. Ding, Z. Yao, T. Pu, P. Zhang, Z. Huang, C. Wang, J. Zhang, N. Zecher-Freeman, H. Zong, D. Yuan, S. Deng, R. Shahbazian-Yassar and C. Wang, Nat. Commun. 13 (2022) 1375.
12. S. Gisbertz, S. Reischauer and B. Pieber, Nat. Catal. 3 (2020) 611-620.
13. J. A. Terrett, J. D. Cuthbertson, V. W. Shurtleff and D. W. C. MacMillan, Nature 524 (2015) 330-334.
14. D. Wang and D. Astruc, Chem. Rev. 115 (2015) 6621-6686.
15. W. J. Kang, B. Li, M. Duan, G. Pan, W. Sun, A. Ding, Y. Zhang, K. N. Houk and H. Guo, Angew. Chem. Int. Edit. 61 (2022) e202211562.
16. C. Han, P. Meng, E. R. Waclawik, C. Zhang, X. H. Li, H. Yang, M. Antonietti and J. Xu, Angew. Chem. Int. Edit. 57 (2018) 14857-14861.
17. G. Brieger and T. J. Nestrick, Chem. Rev. 74 (1974) 567-580.
18. C.-H. Hao, X.-N. Guo, Y.-T. Pan, S. Chen, Z.-F. Jiao, H. Yang and X.-Y. Guo, J. Am. Chem. Soc. 138 (2016) 9361-9364.
19. E. M. Zahran, N. M. Bedford, M. A. Nguyen, Y.-J. Chang, B. S. Guiton, R. R. Naik, L. G. Bachas and M. R. Knecht, J. Am. Chem. Soc. 136 (2013) 32-35.
20. E. Zhao, M. Li, B. Xu, X. L. Wang, Y. Jing, D. Ma, S. Mitchell, J. Pérez-Ramírez and Z. Chen, Angew. Chem. Int. Edit. 61 (2022) e202207410.
21. C. Han, L. Du, M. Konarova, D.-C. Qi, D. L. Phillips and J. Xu, ACS Catal. 10 (2020) 9227-9235.
22. T. Jia, D. Meng, R. Duan, H. Ji, H. Sheng, C. Chen, J. Li, W. Song and J. Zhao, Angew. Chem. Int. Edit. 62 (2023) e202216511.
23. G. Ou, Y. Xu, B. Wen, R. Lin, B. Ge, Y. Tang, Y. Liang, C. Yang, K. Huang, D. Zu, R. Yu, W. Chen, J. Li, H. Wu, L.-M. Liu and Y. Li, Nat. Commun. 9 (2018) 1302.
24. L. Chen, J. Duan, P. Du, W. Sun, B. Lai and W. Liu, Water Res. 221 (2022) 118747.
25. J. J. Houser and B. A. Sibbio, J. Org. Chem. 42 (1977) 2145-2151

Graphical abstract

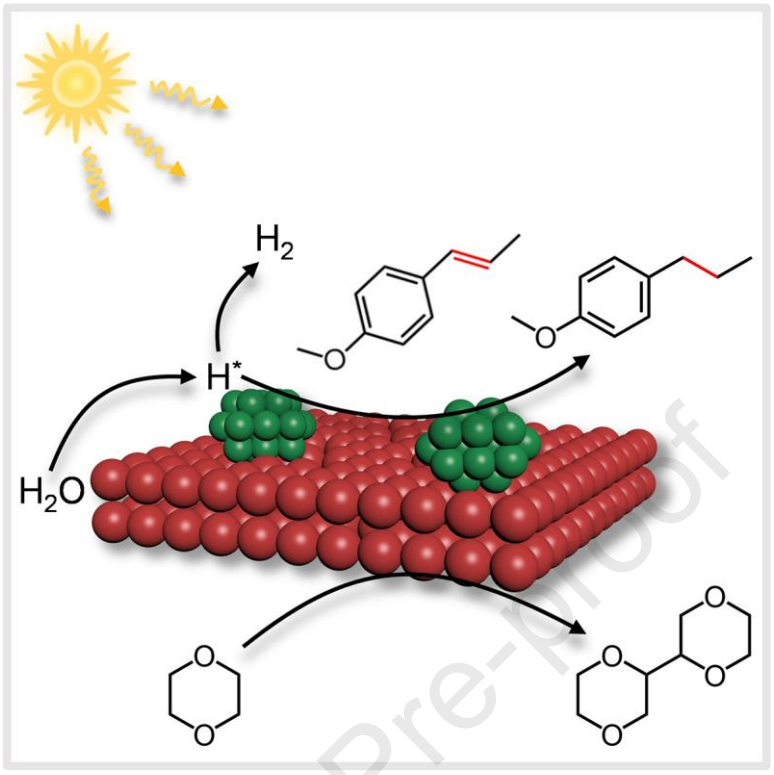

We report an oxygen-defective TiO_2-supported palladium catalyst for efficient photocatalytic transfer hydrogenation using water as the proton source, which exhibits high functional group tolerance and broad substrate applicability, enabling the complete conversion of sixteen substrates.

- An oxygen-defective TiO_2-supported palladium catalyst were prepared by H_2-pretreatment and impregnation for efficient photocatalytic transfer hydrogenation using water as the proton source.

- The optimized system exhibited superior catalytic performance for transfer hydrogenation of anethole using water as a proton source with a 99.9% yield of 4-n-propylanisole formation.

- The photo(electro)chemical analyses demonstrated that the introduction of the surface defects could enhance light absorption and inhibit carrier recombination.

- The reaction mechanism was revealed by isotope-labeling techniques and electron paramagnetic resonance measurements.

Declaration of interests

☒ The authors declare that they have no known competing financial interests or personal relationships that could have appeared to influence the work reported in this paper.

☐ The author *Click here to enter your name* is Choose an item for *Click here to enter the journal's name* and was not involved in the editorial review or the decision to publish this article.

☐The authors declare the following financial interests (e.g., any funding for the research project)/personal relationships (e.g., the author is an employee of a profitable company) which may be considered as potential competing interests:

Click here to enter your full declaration